A novel approach for 3D discrete element modelling the progressive delamination in unidirectional CFRP composites

A novel approach for 3D discrete element modelling the progressive delamination in unidirectional CFRP composites

Lei Wan[a,b], Yong Sheng[c], Edward D. McCarthy[a], Dongmin Yang[a,*]

[a]*School of Engineering, Institute for Materials and Processes, The University of Edinburgh, UK*
[b]*School of Mechanical and Aerospace Engineering, Queen's University Belfast, UK*
[c]*Faculty of Science and Engineering, University of Wolverhampton, UK*

Abstract

This study proposed a novel approach based on the 3D discrete element method (DEM) to simulate the progressive delamination in unidirectional carbon fibre reinforced polymer (CFRP) composite laminates. A hexagonal packing strategy was used for modelling 0° representative plies, the interface between different plies was modelled with one bond and seven bonds following the conservation of energy principle and a power law. The number of representative layers and the stiffness of bonds within these layers were calibrated with a comparison of results obtained from finite element method and theoretical analysis. DEM simulations of delamination with both interface models were conducted on unidirectional composites for double cantilever beam (DCB), end-loaded split (ELS) and fixed-ratio mixed-mode (FRMM) tests. It was found that the seven-bond interface model has a better agreement with experimental data in all three tests than the one-bond interface model by adopting the proposed seven-bond arrangement in terms of the progressive delamination process. The main advantages of the present interface model are its simplicity, robustness and computational efficiency when elastic bonds are used in the DEM models.

Key words: Carbon fibre reinforced polymer composite (CFRP); Discrete element method (DEM); Delamination; Conservation of energy principle; Critical fracture energy

*Corresponding author
Email addresses: Dongmin.Yang@ed.ac.uk (Dongmin Yang)

1. Introduction

Advanced Carbon Fibre Reinforced Plastic (CFRP) composite materials are widely used in various industries including aerospace, automotive and renewable energy due to their excellent stiffness- and strength-to-weight ratios, corrosion resistance and flexibility of structural optimisation for economic and environmental reasons. However, the lack of understanding of composite failure mechanisms under complex loading conditions imposes a challenge for engineers for the design and optimisition of composite structures. Among composite failure modes, interlamina delamination is regarded as the most significant issue in CFRP composites, which occurs at the weakest region in the composite where the matrix is rich and results in significant stiffness and/or strength degradation. Therefore, high-fidelity modelling of the interface is of great significance for accurate predictions of damage initiation and propagation in CFRP composite materials.

Finite Element Modelling (FEM) is widely used for predicting damage initiation and progression in composites, usually associated with the fracture mechanics approach or cohesive zone models. The Virtual Crack Closure Technique (VCCT) [1, 2, 3, 4] and Cohesive Zone Models (CZM) [5, 6, 7, 8], including the Discrete Cohesive Zone Model [9] and the Discrete Damage Zone Model [10] are well studied for the prediction of delamination damage onset and propagation. The VCCT determines the Energy Release Rate (ERR) at the crack ahead by using forces and displacements obtained from the FE model. An assumption is needed when modelling the delamination damage growth that the energy released during crack growth is equal to the energy required to close the crack back to its original length [1]. This technique can predict the delamination accurately to some extent, however, it requires knowledge of the pre-defined delamination path prior to damage [7] and also it assumes self-similar damage growth [11]. Meanwhile, the potential for non-convergence still exists due to the singular finite element stiffness matrices[12, 11, 7].

The aforementioned approaches based on FEM suffer from the meshing issue, especially when the occurrence of fracture results in mesh deleting. Therefore, these mesh-dependent approaches require a costly remeshing strategy to alleviate such effects [6]. There is another

class of numerical methods qualified as meshless methods, which can simulate the crack propagation without the consideration of the crack's topology [13]. Two meshless numerical methods have been reported for the failure prediction of composite materials, namely peridynamics [14, 15] and discrete element method (DEM) [16, 17]. The peridynamics approach adopts an integral formulation to describe continuous problems while it avoids classical issues related to partial differential equations occurring in FEM. Forces applied to a particle are estimated by summing the contributions from all the particles around it in a certain region. The larger the region that is chosen, the more accuracy is obtained. DEM was originally used in the field of rock mechanics [16], which shares several similarities with the peridynamics approach as the motion of a particle is calculated based on Newton's second law and uses the forces acting on it from surrounding particles. However, DEM adopts a different modelling strategy compared with peridynamics, in which all particles in the DEM-based model are modelled as individual entities and calibration for their microscopic parameters (i.e. stiffness and strength), is usually required, especially when the particles are randomly packed or arranged in a complex layout.

In the last decades, DEM has attracted increasing attention in the composite communities due to its capability of capturing damages and their growth in the composite materials without any preset paths [18]. For example, crack initiation and propagation in composite materials were simulated by DEM models under various loading conditions at different scales [19, 20, 21, 22, 23], which demonstrate the capability of DEM in the prediction of cracks in composites with details of crack density and stiffness reduction. Yang et al. [24] proposed a 2D DEM model to model progressive delamination of laminated composites, in which the anisotropic composite plies were constructed with a hexagonal packing strategy while the interface between plies was modelled by a contact softening model with a bilinear elastic behaviour. Good agreements were observed between the DEM and existing numerical and experimental results in terms of the double cantilever beam (DCB), end-loaded split (ELS) and fixed-ratio mixed-mode (FRMM) tests. However, it was limited to the 2D DEM modelling of the progressive delamination of composites, which cannot capture the delamination in three dimensions for angle-ply composites and the interaction of different damage

modes. Meanwhile, due to the softening behaviour considered in every single bond with the contact softening model in [24], the computational cost could be much higher than the one which uses the linear elastic brittle model. More recently, Le et al. [25] developed a 3D DEM model to capture several damage modes in composite materials, such as fibre/matrix debonding, matrix cracking, fibre breakage and delamination. In the 3D DEM model, matrix and fibres were modelled as brittle materials, in which two failure criteria were used for comparison, i.e. a breakable bond failure criterion and a removed discrete element failure criterion; while the interfaces between fibres and matrix and different plies were modelled by cohesive contact models [26], in analogy to the cohesive zone model in FEM. Due to the random arrangements of the particles and bonds, calibration of microscopic parameters (i.e. the radius of particles, Young's modulus and Poisson's ratio) were conducted for the DCB test by i) determining the radius of particles with arbitrarily selected Young's modulus and Poisson's ratio and ii) determining the microscopic Young's modulus and Poisson's ratio with the calibrated radius of particles. Ammar et al. [27] applied a similar bond constitutive model with bilinear softening law to capture the delamination in DCB, ELS and MMB tests. However, the interface was modelled with randomly distributed bonds, inevitably increasing the computational cost.

In this paper, a novel approach is proposed to model the interlaminar interface of unidirectional composites with a seven-bond interface model based on DEM, aiming to capture the progressive delamination process. This approach used elastic brittle bonds with a specific pattern, instead of the exclusive use of cohesive/softening bonds, to capture the progressive delamination of composites by the progressive bond breaking events. The fracture criterion is stress-based, in which the strength of interface bond is determined by the critical energy release rate within the framework of fracture mechanics. The relation of the fracture energy stored in different types of bonds within one unit can be represented by the length of the bonds based on a power law. This approach can be also extended to the prediction of delamination in angle-ply composites and provides guidance for other meshless bond-based lattice models (i.e. peridynamics [28]) for modelling interlaminar interface. This paper is organised as below. The general concept of the DEM theory is first recalled, followed by a

discussion of the modelling of the unidirectional composite lamina with a hexagonal packing method. The DEM models of the composite interlaminar interface were built up with a newly proposed approach, in which the stiffnesses and strengths of bonds were determined based on the ERR concept. Numerical analysis of DCB, ELS and FRMM tests was conducted on unidirectional CFRP composites and validated against experimental data in the literature.

2. DEM modelling of composite lamina

DEM was originally proposed by Cundall [16] to simulate the movement and interaction of rigid particles assemblies in the context of rock mechanics and has been extended to other fields, such as concrete [29], ceramics [30] and fibre reinforced polymer composite [25, 23]. In a typical DEM model of a solid, the particles are assumed to be rigid spheroid in a 3D or disc in 2D, in which the interaction between the contacting particles is treated as a dynamic process and the stress and deformation of the particle assembly are obtained from the force and displacement of each individual particle. The translational and rotational motion of a single, rigid particle is determined by the resultant force and moment vectors acting upon it. The contact forces and displacements of the assembled particles can be recorded by tracing the movements of the individual particles. In a typical cycle of calculation, the forces/moments and displacements are exchanged between Newton's second law and a force-displacement law. The position and velocity of each particle are updated according to Newton's laws of motion in the current timestep and the forces/moment calculated during the previous timestep, while the forces/moments developing at each contact are updated by an appropriate contact model using the current state of the particles.

Particles are usually bonded at contacts when the surface gap between the two particles is less than or equal to zero and separated when the bond stress exceeds its strength. The advantage of this method is that the crack can be tracked at the contact point when the bond breaks. The mechanical behaviour of bond-based DEM model is largely dependent on the contact model which updates the forces and moments. Here in this study, the parallel bond contact model, is selected to describe the mechanical behaviour of the bonds at contact. As

shown in Fig. 1, the components and parameters of the parallel bond model in normal and shear directions are illustrated, in which $\overline{k}_n$ and k_n are the normal stiffness of the parallel bond and particles, respectively. g_s and $\overline{\sigma_c}$ are the surface gap between two particles and the tensile strength of the bond, respectively. $\overline{k}_s$ and k_s are the shear stiffness of the parallel bond and particles, respectively. μ is the friction coefficient between two particles, and the $\overline{\Phi}$ and $\overline{c}$ are the friction angle and cohesion stress, respectively, in the failure curve of the parallel bond subjected to tension/compression and shear stresses. In the DEM model

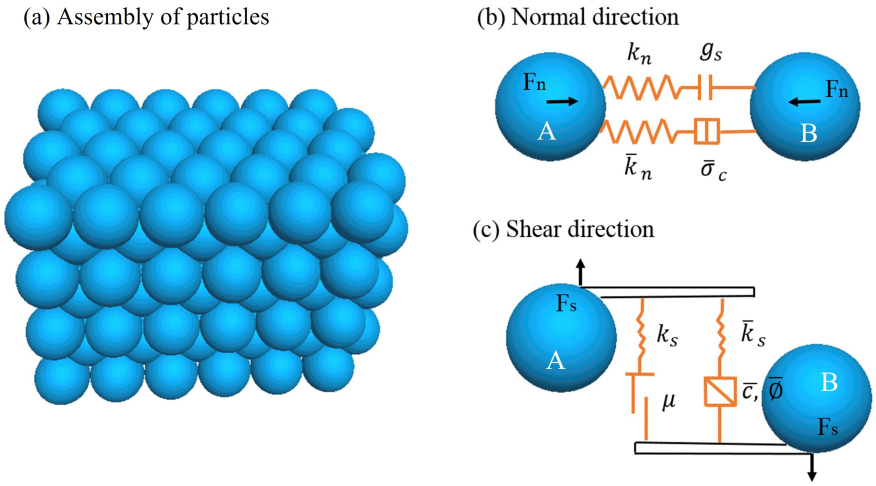

Figure 1: Parallel bond in DEM modelling

constructed with parallel bonds, the contact stiffness, K_i, at the particle-particle contact can be obtained from the stiffnesses of particles and parallel bonds [31],

$$K_i = A\bar{k}_i + k_i \tag{1}$$

$$A = 2\bar{R}\delta \tag{2}$$

$$K_i = \frac{k_i^{[A]} k_i^{[B]}}{k_i^{[A]} + k_i^{[B]}} \tag{3}$$

where $\bar{R}$ and A are the radius and cross-section area of the parallel bond, respectively. δ is the element thickness, $\bar{k}_i$ is the parallel bond stiffness and k_i is the equivalent stiffness of the two contacting particles. i is in place of n or s, which indicates normal or shear direction, respectively.

In our previous work [32, 23], an extended 2D DEM model with the hexagonal packing method was successfully applied to construct unidirectional composites. In the extended 2D DEM model of a composite lamina, the basic unit comprises seven particles, in which one particle is located in the centre of the unit and the surrounding particles are packed in a hexagonal pattern. The parallel bonds aligned with the fibre direction are called *fibre bonds* and the remaining bonds in blue are called *matrix bonds*. The angle of the lamina is dependent on the direction of the *fibre bonds*. The stiffnesses of the *fibre bonds* and *matrix bonds* are determined by the average strain energy method [33], while the strengths are calibrated from the experimental data.

The constitutive law of the parallel bond is defined by a relationship between the traction and the relative displacement at the interface, see Fig. 2. The fracture criterion of interface bonds is based on the ERR concept. Since the bond-based DEM model implies the absence of stress singularities at the crack tip, the ERR in an interface model can be defined as the elastic strain energy per unit length stored in the unbroken bonds at the crack tip [34, 35]. In the constitutive model , the normal stress increases with the elongation of the bond between two adjacent particles and reduces to zero when it exceeds the corresponding strength $\overline{\sigma}_{nc}$. It should be noted that the normal strength $\overline{\sigma}_{nc}$ is calculated from the critical fracture energy G_{IC}, i.e. the grey triangle area in Fig. 2(a). The normal stress is calculated from $\overline{\sigma}_n = \frac{\overline{F}_n}{\overline{A}}$. The bond is deleted when the normal stress exceeds the strength and no longer holds stress between two particles, which is found in Fig. 2(b). The shear strength $\overline{\sigma}_{sc}$ and stress $\overline{\sigma}_s$ of the bonds are calculated from critical fracture energy G_{IIC} and force $\overline{F}_s$ in the tangential direction, respectively. The constitutive model of the bonds in the tangential direction for the undamaged and damaged interface can be seen in Fig. 2(c) and (d), respectively. Here in this study, Double Cantilever Beam (DCB), End Loaded Split (ELS) and Mixed Mode Bending (MMB) tests are studied with a newly proposed seven-bond interface model and previously reported one-bond interface model.

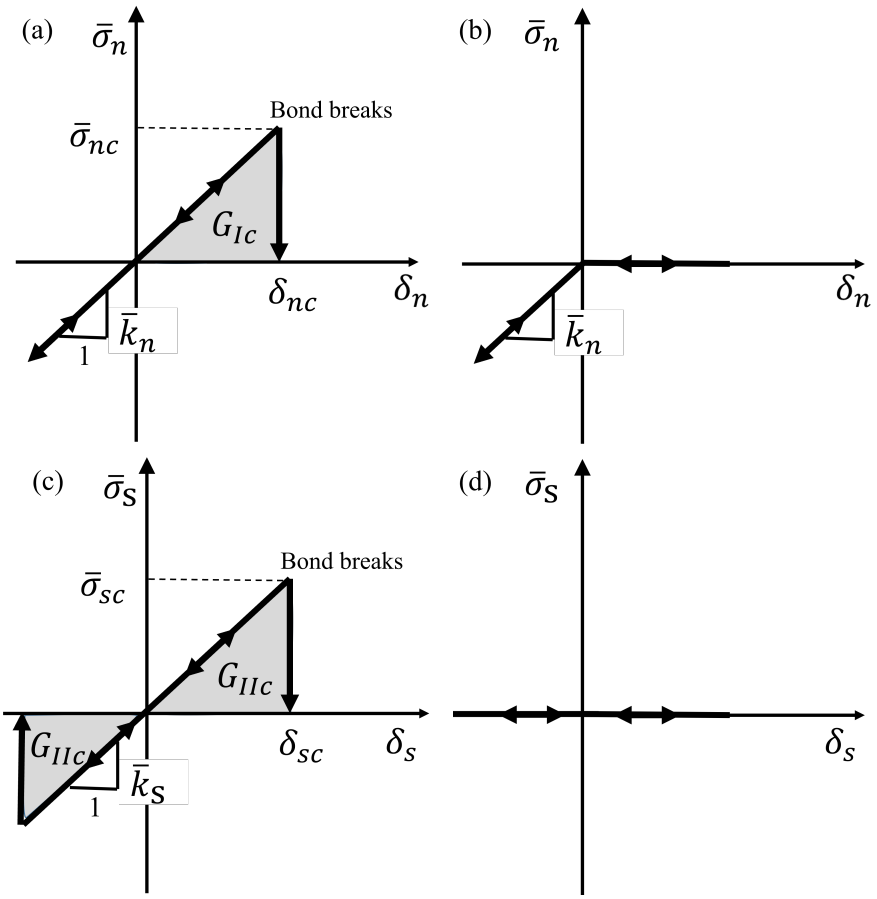

Figure 2: Linear elastic brittle law of the parallel bond in the normal direction for (a) an undamaged interface and (b) a broken interface, and in the tangential direction for (c) an undamaged interface and (d) a broken interface [36].

2.1. DEM modelling of delamination in unidirectional composites

2.1.1. One-bond interface model

In the previous DEM models, the particles in the adjacent two plies are mirrored about the interface, thus the particle in one ply is only bonded to the mirrored particle in the other ply. This model is named as a one-bond interface model. The illustration of the one-bond interface is seen in Fig. 3(a), in which the red vertical bonds represent the interface between two plies. The critical fracture energy G_{IC} and G_{IIC} are related to the effective ultimate

nominal traction $\overline{\sigma}_{nc}$ and $\overline{\sigma}_{sc}$ of material and the final separation δ_{nc} and δ_{sc}, respectively.

$$G_{IC} = \frac{\overline{\sigma}_{nc}\delta_{nc}}{2} \tag{4}$$

$$G_{IIC} = \frac{\overline{\sigma}_{sc}\delta_{sc}}{2} \tag{5}$$

Since the damage model is brittle, so the bond stiffness $\overline{k}_n$ and $\overline{k}_s$ can be calculated from the final separation δ_{nc} and δ_{sc} via

$$\overline{k}_n = \frac{\overline{\sigma}_{nc}}{\delta_{nc}} \tag{6}$$

$$\overline{k}_s = \frac{\overline{\sigma}_{sc}}{\delta_{sc}} \tag{7}$$

The critical fracture energy G_{IC} and G_{IIC} can be obtained from the corresponding DCB and ELS experiments, respectively. Therefore, the ultimate nominal traction can be determined from

$$\overline{\sigma}_{nc} = \sqrt{2\overline{k}_n G_{IC}} \tag{8}$$

$$\overline{\sigma}_{sc} = \sqrt{2\overline{k}_s G_{IIC}} \tag{9}$$

It is reasonable to assume that the relationship between the critical strain energy release rate in mode I and mode II is linear when subjected to a mixed-mode loading condition [37, 38]. Thus a linear fracture criterion for mixed-mode loading is adopted:

$$\frac{G_I}{G_{IC}} + \frac{G_{II}}{G_{IIC}} = 1 \tag{10}$$

where G_I and G_{II} are the strain energy release rate of mode I and mode II, respectively. Here a mixed-mode FRMM test was used for the numerical simulations of mixed mode fracture. The ratio of mode I to mode II loading is approximately constant throughout the test at 4:3 [39], resulting in the value of G_I/G_{II} as 1.33.

2.1.2. Seven-bond interface model

Different from the one-bond interface model, each particle is connected with seven bonds within a unit region in the seven-bond interface model. The configuration of the interface

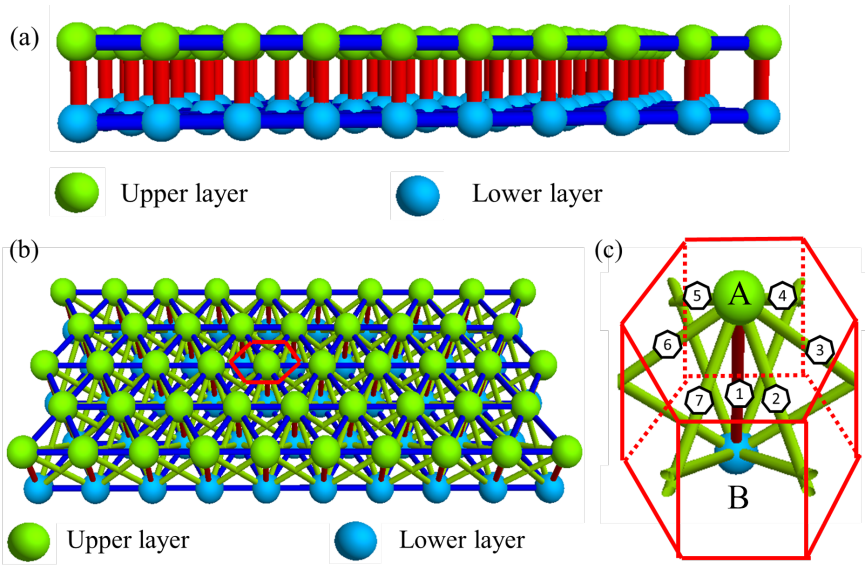

Figure 3: (a) One-bond interface DEM model, (b) seven-bond interface model and (c) configuration of bonds in one unit of seven-bond interface model.

is illustrated in Fig. 3(b-c), in which particle A connects not only with the counterpart particle B, but also the other six particles surrounding particle B. Therefore, considering the conservation of energy principle, the whole critical fracture energy can be spread into seven parts, which represent the fracture energy of the primary vertical bond (G_I) and the surrounding softening bonds ($G_i(i = 2, 3...7)$), respectively. Thus the whole fracture energy can be written as:

$$G_{IC} = G_1 + \Sigma G_i, (i = 2, 3...7) \tag{11}$$

The relation between G_1 and G_i can be established based on the relation of the length of these bonds by using a power law:

$$G_1 = A(\frac{L_i}{L_1})^B G_i, (i = 2, 3...7) \tag{12}$$

where A and B are two factors influencing the relation between G_1 and G_i. L_1 and L_i are the length of the primary vertical bond and surrounding softening bonds, respectively. According to the spatial location of these bonds in Fig. 3(c), the ratio between the L_i and L_1 is $\sqrt{2}$. This ratio can be adjusted for other composite laminae according to the configuration of the packed particles.

3. Determination of packing strategy and bond stiffness

Before carrying out numerical simulations of DCB tests, it is necessary to determine the radius of particles used for the configuration of the DEM model. In order to be in accordance with the DCB specimen in the literature [40], the size of the specimen size for the cantilever test is 64.8 mm × 10 mm × 1.62 mm, with a length of 1 mm for loading on the left (blue balls) and a length of 13.8 mm on the right (red balls), resulting in an effective length of 50 mm. The schematic and configuration of the cantilever constructed by DEM can be found in Fig. 4. The material properties of this specimen [40] are: longitudinal Young's Modulus E_1=130 GPa, transverse Young's Modulus E_2=6.5 GPa, shear modulus G=2.7 GPa, and mode-I critical energy release rate G_{IC} = 643 J/m^2.

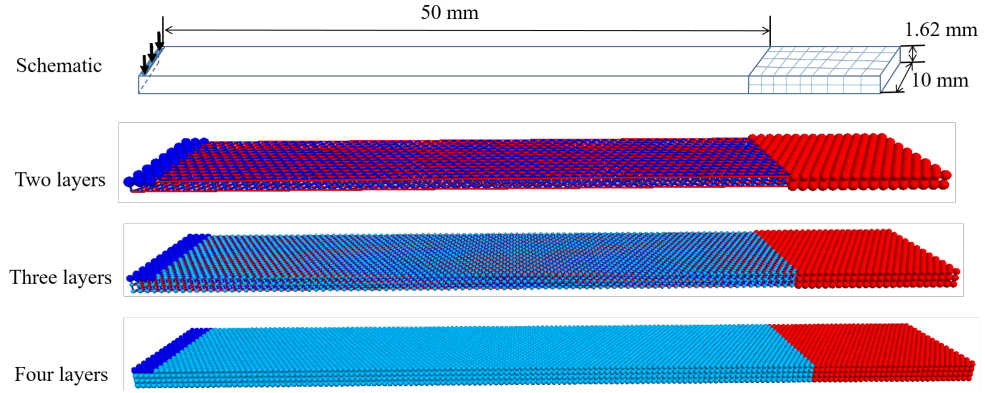

Figure 4: Layups of UD laminate with different configurations for the cantilever test. (The particles in the DEM model with two layers are hidden, the radius of particles is reduced to half of its original size in the one with three layers model and no change is made in the one with four layers for interpretation.)

It was assumed that there is no intralaminar and interlaminar damage occurring in the specimen for the determination of bond stiffnesses. A convergence study was conducted on the number of representative layers of the specimen and numerical results are listed in Table 1. The initial stiffness of the parallel bond at the interface of these representative layers of the specimen is determined by $\overline{k}_n = E_2/2R$ [31]. The diameter of particles was determined by dividing the composite thickness, which is 1.62 mm in this case, into the number of representative layers. The velocity 0.1 m/s [24, 32] was applied to the blue loading

particles in a vertical direction, and the red particles were fixed. The bending stiffness of this cantilever was obtained by averaging the unbalanced force of the blue particles in the loading direction when their displacements reach 1 mm. It can be found in Table 1 that the stiffness of the cantilever predicted by the DEM model with three representative layers becomes converged with a reasonable computational cost, compared to the other models. The computer used for the numerical simulations is a PC with 8-core Intel E5-2670 (2.6 GHz) processors and 16 GB of memory and the typical DEM simulation time ranges between 8-24 hrs depending on the composite structures and boundary conditions. Therefore, three representative layers were selected for the construction of the DEM models in DCB, ELS and FRMM tests.

Table 1: The dimension and obtained results of cantilever DEM model with different configurations

	Two layers	Three layers	Four layers
Particle diameter 2R (mm)	0.81	0.54	0.405
Representative layer arrangement	$80 \times 15 \times 2$	$120 \times 23 \times 3$	$160 \times 60 \times 4$
Bending stiffness (N/mm)	17.47	24.05	23.90
Computation time (min)	7	45	100

It is extremely difficult to acquire a microscale parameter such as interface stiffness from an experiment. In the simulation of the DCB test with FEM, an empirical penalty stiffness is usually chosen for the stiffness of the cohesive zone model to maintain its continuity of stress and strain between different parts [41]. Here, in this case, a parametric study was conducted for the determination of interface stiffnesses of DEM models with three representative layers, starting from the base value of 12000 GPa/m ($E_2/2R$). Comparing the numerical results obtained from the DEM models, it can be found that the bending stiffness decreases as the bond stiffness decreases. With a comparison of predicted bending stiffness obtained from DEM and FEM simulations as well as beam theory, the bond stiffness of 1200 GPa/m was found to be in good agreement with FEM and theoretical predictions, see Table 2. Therefore, 1200 GPa/m was selected for the DCB test in the next section.

Table 2: Comparison of numerical results obtained from DEM and FEM models with theoretical prediction

	$\overline{k}_n$ (Pa/m)	Bending stiffness (N/mm)
DEM model	1.2×10^{13}	24.05
	0.6×10^{13}	20.35
	1.2×10^{12}	12.81
	1.2×10^{11}	5.62
FEM model	-	11.77
Beam theory	-	11.85

4. Modelling DCB test of unidirectional composites

The DCB test of CFRP composite laminates was conducted with the aforementioned two interface models and the numerical results were compared to the experimental findings [40]. The configuration and dimensions of the specimen are shown in Fig. 5(a), in which the total length (L) is 180 mm, the width is 20 mm, the initial length of the crack (a_0) is 50 mm and the total thickness ($2h$) is 3.24 mm. Here in order to reduce the computational cost, the

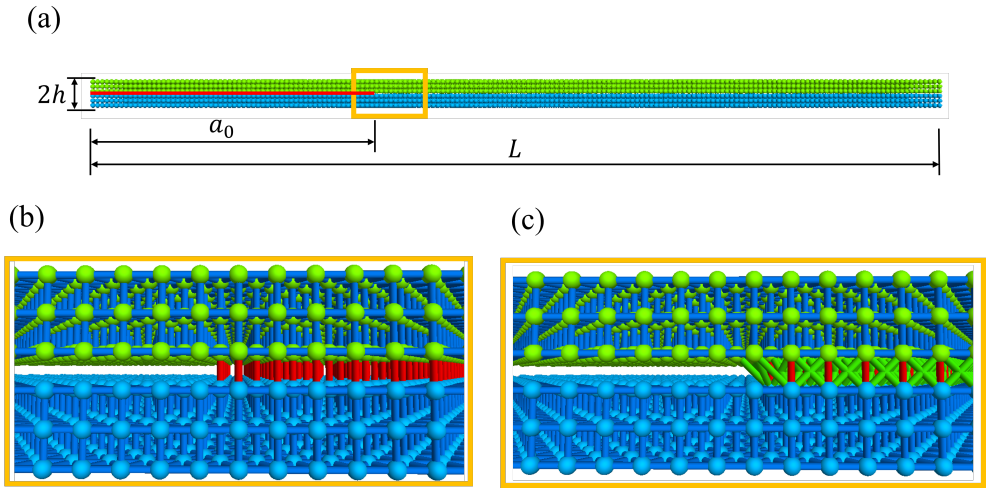

Figure 5: Configuration of DCB specimen: (a) sketch of DCB specimen, (b) one-bond interface model, (c) seven-bond interface model. (The radius of particles of DEM models is reduced to half of its original size for interpretation, and bonds are illustrated as coloured cylinders.)

width of the DEM models was reduced to 10 mm. In both models, a total of six plies were used, making the particle diameter 0.54 mm, with the upper and lower laminates consisting of three representative layers. The strength of bonds in upper and lower representative layers was set to be extremely high to prevent any breakage, shown as blue in Fig. 5(b-c). The strength of bonds at the DCB interface in the one-bond interface model was determined using Eq. 8, while the strengths of bonds at the DCB interface in the seven-bond interface model were determined by Eqs. 8 - 12.

In order to study the influence of stiffness on the numerical results of the DCB test, three stiffnesses, 120 GPa/m, 1200 GPa/m and 12000 GPa/m were selected and the strength of the interface bonds was calculated from Eq. 8. The comparison of force-opening displacement curves obtained from DEM simulation and experiment are shown in Fig. 6(a). During the elastic stage, the numerical simulation curves with the stiffness of 1200 GPa/m and 12000 GPa/m, are in good agreement with the experimental curve. When the opening distance is larger than 4 mm, the bonds of the interface between upper and lower layers start to hold the load, resulting in fluctuations in the curve. It is found that the result obtained from the model with 1200 GPa/m interface stiffness is in excellent agreement with the peak load obtained from the experiment [40], while the results obtained from the ones with the interface stiffness of 120 GPa/m and 12000 GPa/m were slightly underestimated and overestimated, respectively. When the displacement increases beyond 7.2 mm, the interface bonds start to break, resulting in a decrease in loading force and noticeable fluctuation during crack propagation. A good match can be observed between numerical simulation and experiment during the post-peak cracking process.

The stiffness of interface bonds in the seven-bond interface model are selected as 1200 GPa/m, and the strengths of these bonds are calculated according to Eqs. 8 - 12. The comparison of force-opening displacement curves between numerical results obtained from the seven-bond interface model and the experimental result can be found in Fig. 6(b-c). Since the parameter B has a significant influence on the strengths of the primary bond and softening bonds, the parametric study for the determination of B was carried out with the parameter $A = 1$. It can be seen from Fig. 6(a) that all of the curves are superposed before

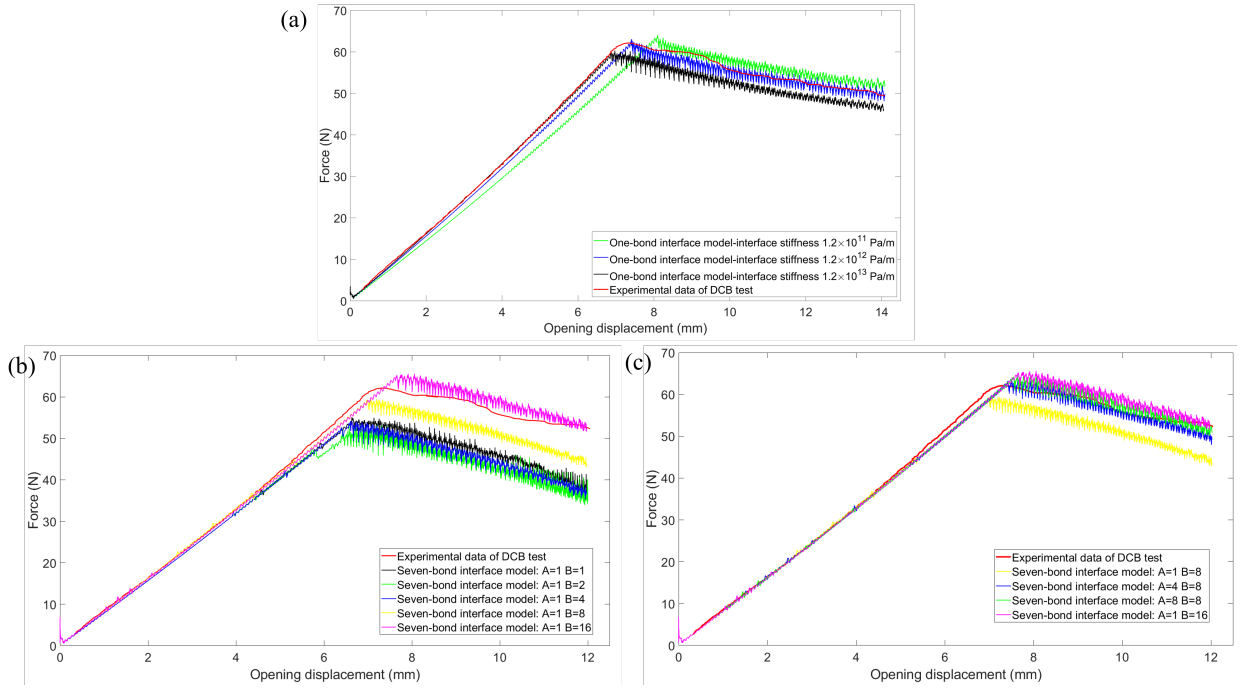

Figure 6: Comparison of force - opening displacement curves between the experiment [40] and numerical results obtained from (a) one-bond interface model, (b) seven-bond interface model with A=1 and (c) seven-bond interface model with B=8.

the opening displacement of 4 mm during the elastic stage. As the opening displacement increases, the softening bonds start to break, resulting in a slight drop in the curves, while the primary bonds still hold the load until their breakage at the peak load, see the curves obtained from $B = 2$ and 4. The peak load increases as the parameter B increases, since a larger primary strength can be obtained from a larger B. Spurious oscillation can be observed in all the cases regarding the reaction force, after the peak reaction force when primary bonds start to break. The fluctuations occurring during progressive delamination process are related to the explicit dynamic simulations and require a high damping and fine time steps to be mitigated. It can be seen in Fig. 6(b) that the seven-bond interface model with the parameter $B = 16$ overestimates the peak load, thus a parametric study to determine the parameter A was conducted with the parameter B of 8. The curve obtained from the model with $A = 4$, $B = 8$ is in excellent agreement with the experiment [40] both in the elastic stage and during the cracking propagation process, which demonstrates the

capability of this seven-bond interface model regarding cracking prediction in the DCB test.

Fig. 7 shows the comparison of cracking length-opening displacement between the two interface models and experiment data [40]. For the seven-bond interface model, solid lines represent the length of a primary zone where the current crack tip can reach during cracking propagation, while the dash lines represent the length of the softening zone, and the gap between these two lines represents the processing zone, see Fig. 7. It was found that with the parameter $B = 8$ and 16, the cracking length of softening zone starts from around 55 mm, this is due to the data saving frequency, and the cracking information can only be recorded at a prescribed timestep. The opening displacement obtained from the numerical results with $A = 4$, $B = 8$ shows excellent agreement with the one obtained from the experiment, which can be also proved by the force-opening displacement curve in Fig. 6(c). However, during the cracking propagation after the opening displacement of 9 mm, the numerical result obtained from $A = 1$, $B = 4$ has a reasonable agreement with the experiment. The numerical result obtained from the one-bond interface model overestimates the opening displacement at the cracking onset and underestimates the cracking length during the propagation process. Interestingly, no processing zone, which depicts the difference between the cracking region of softening bonds and primary bonds, can be found in this case during the cracking process, see Fig. 7(b) when $A = 1$, $B = 4$, that is due to the slight difference between the strength of the primary bond and softening bonds.

5. Modelling ELS test of unidirectional composites

An ELS test was carried out with a constant velocity of 0.1 m/min applied on the left edge of a specimen composed of 18 018 particles and 63 443 bonds (Fig. 8(a)). The geometry of the specimen is characterised by the following dimensions in Fig. 8: length L=105 mm, width B=24 mm, thickness $2h$= 3.05 mm and pre-crack a_0=60 mm. The diameter of the particle is determined by the thickness of the specimen and the selected number of layers. In addition, the material properties of this specimen [24, 42] are: longitudinal Young's Modulus E_1=130 GPa, transverse Young's Modulus E_2=8 GPa, shear modulus G=6 GPa, mode-II critical energy release rate $G_{IIc} = 856\ J/m^2$ and interfacial strength τ= 48 MPa.

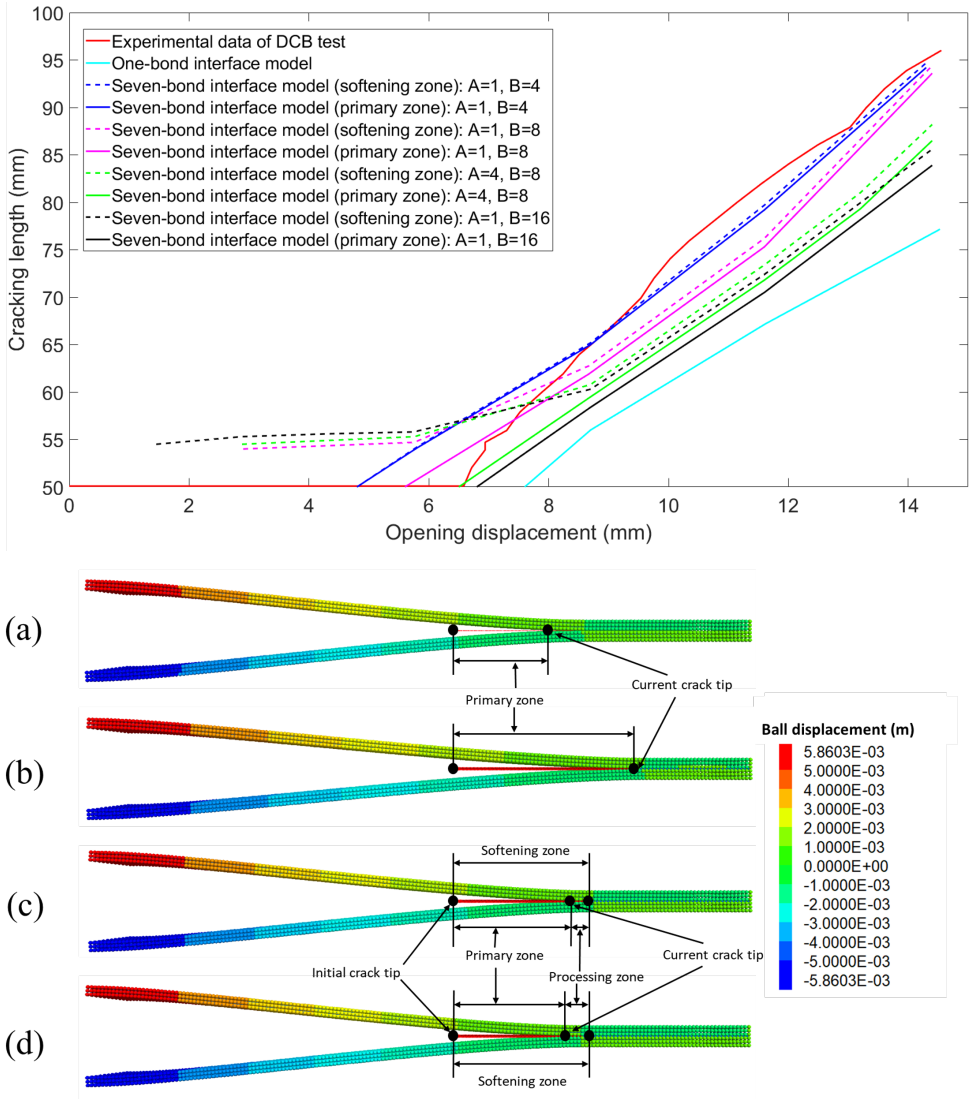

Figure 7: Comparisons of cracking length-opening displacement curves between different interface models and experiment [40], and cracking propagation of (a) one-bond interface model and seven-bond interface models (b) A=1, B=4, (c) A=4, B=8, (d) A=1, B=16 at the opening displacement of 11.6 mm.

All discrete particles are connected by parallel bonds. The interfaces in the upper and lower representative layers, depicted with green and blue particles in Fig. 8(a), respectively, are connected with one bond. The stiffnesses of these interface bonds are calibrated compared to the analytical result [42] with an assumption that normal and shear stiffness are equal, and the strengths are assumed to be infinite to avoid failure. The interface between upper and lower layers is modelled with one bond and seven bonds, respectively. The stiffness

of the interface bonds is calculated using Eq. 8 from the critical energy release rate and interfacial shear strength.

It was found from the force-end displacement curves in Fig. 8(b) that the slope of the curves increases as the bending stiffness of the representative layers increases. A bond stiffness of 53.8 GPa/m was found to agree excellently well with the analytical result [42]. The fluctuations in the elastic stage found on all curves are probably due to the elastic wave passing through the interface region before it becomes stable. An interface shear strength of 48 MPa was found to be larger in the numerical simulation compared to the experimental result [42], which is similar to the numerical result obtained with the seven-bond interface model in Fig. 8(b) when A=1, B=16. The seven-bond interface model with A=1, B=8 agrees reasonably well with the experimental result during the cracking propagation, and the results with A=1, B=2 and A=1, B=4 show no failure when the end displacement reaches 20 mm.

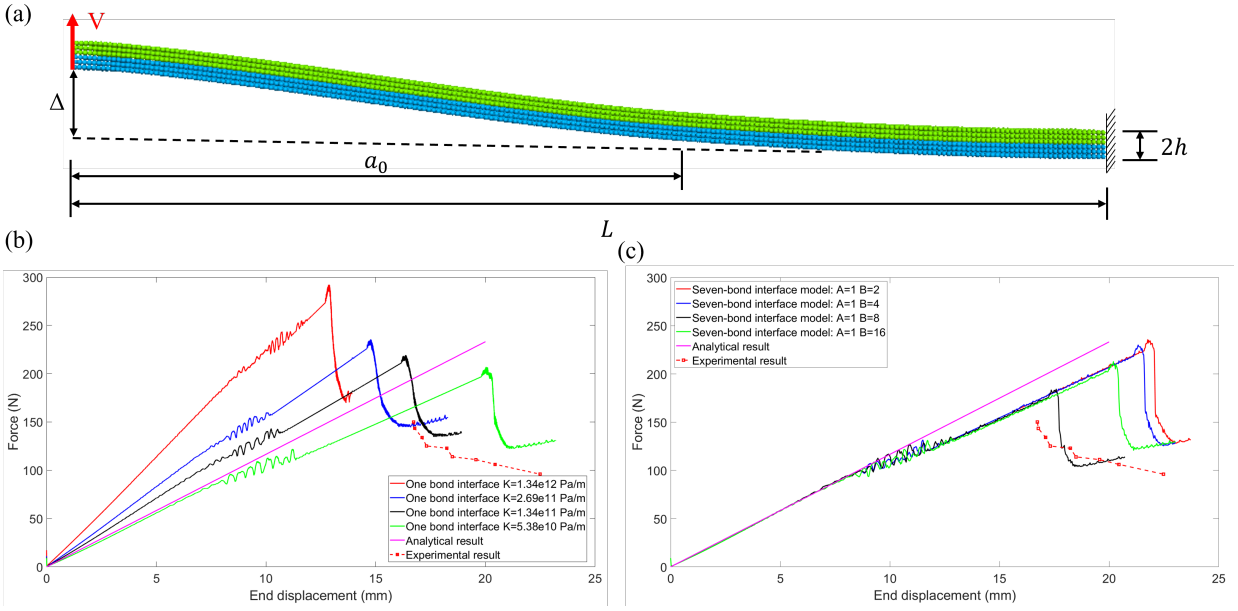

Figure 8: (a) schematic of ELS test and comparison of load-displacement curve from (b) one-bond interface model and (c) seven-bond interface model.

Fig. 9 shows the comparisons of cracking length and cracking disc number against end displacement of the ELS test between one-bond and seven-bond interface models. It can

be seen in Fig. 9 that in the seven-bond interface model with A=1, B=16, the cracking of the softening bond starts when the end displacement reaches about 4 mm (Fig. 9(b)) and the primary bond loses the capability of holding load when the displacement reaches 17 mm and becomes stable at 20 mm (Fig. 9(a)). The same phenomenon was found in the seven-bond interface model with A=1, B=8, where the damage initiates at an end displacement of 10 mm, and an earlier breakage of the primary bond occurs at around 17 mm. For the seven-bond interface model with A=1, B=2 and A=1, B=4, the cracking of softening bonds was delayed until an end displacement of 18 mm. Such delay results in a higher peak load compared to the models with A=1, B=8 and A=1, B=16 (Fig. 8(c)). The one-bond interface model has a similar trend with the seven-bond interface model with A=1, B=16 due to the close strength of its interface bond with the primary bond in the seven-bond model, however, the softening processing cannot be captured by the one-bond interface model.

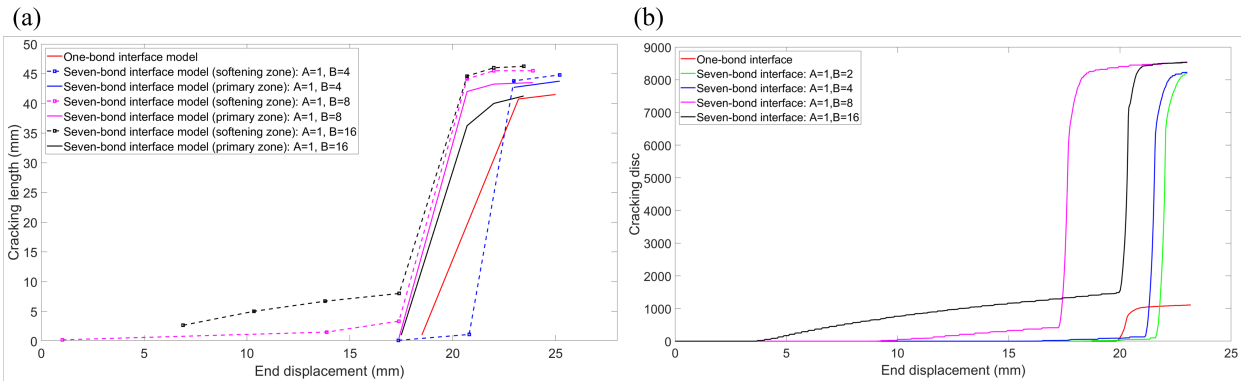

Figure 9: Comparisons of (a) cracking length - end displacement curves and (b) cracking disc number - end displacement of the ELS test between one-bond and seven-bond interface models.

6. Modelling FRMM test of unidirectional composites

The mixed-mode fracture of the interface was studied by the DEM simulation of the FRMM test with one-bond and seven-bond interface models. The mechanical properties of the specimen were the same as the one used in the ELS test, while the pre-crack length of 45 mm was used in the FRMM test. Chen et al. [42] artificially increased the longitudinal Young's modulus to fit the FEM results close to the experiment. Yang et al. [24] conducted

parametric studies of the influences of bond strengths and critical fracture energies on the performance of a bond-based softening model and found the obtained results generally agreed but underestimated the peak load. Here, in this FRMM test, the stiffnesses of the interface of representative layers were calibrated using the approach described in Section 3 and the results were compared with analytical and experimental data [42], see Fig. 10(a). It was found that the stiffness of 538 GPa/m provides an excellent agreement with the analytical result. For simplicity, it was assumed that the critical fracture energy in mode I and mode II are the same as the one in the mixed mode, $G_C = G_{IC} = G_{IIC}$ and the strength of bonds is 48 MPa [24, 42]. It should be noted that the latter value was adopted as a baseline and it underestimates the peak load compared to another softening bond model in DEM [24] and a bilinear cohesive zone model in FEM [42] due to the characteristic of their constitutive models. Thus a parametric study of the bond strength of the interface was conducted, and the bond strength of 60 MPa was found to be slightly larger than that of the experimental result with a similar cracking propagation trend.

The same stiffnesses were used for the interfaces of the representative layers and the specimen in the seven-bond interface model, and the strengths of the primary bond and the softening bonds were calculated according to Eqs. 8 - 12. It was found in Fig. 10(b) that all the simulated results obtained from the one-bond interface model underestimate the peak load compared to the experiment. In Fig. 10(c), the results obtained from the seven-bond model with A=1, B=2 and A=1, B=4 share similar patterns which both agree reasonably well with the experimental curve regarding the cracking propagation process. The model with A=1 and B=8 underestimate the peak load compared to the experimental data. The one-bond interface model generated almost the same curve as the seven-bond interface model with A=1, and B=16 due to their close bond strength. However, the cracking lengths are different due to the faster cracking propagation of softening bonds, see Fig. 10.

Fig. 11 shows the comparison of the cracking length and the cracking disc number against end displacement obtained from the FRMM test with one-bond and seven-bond interface models. Smooth cracking propagation was detected in the comparisons, associated with the force-end displacement curves in Fig. 10(b-c). In the comparison of seven-bond interface

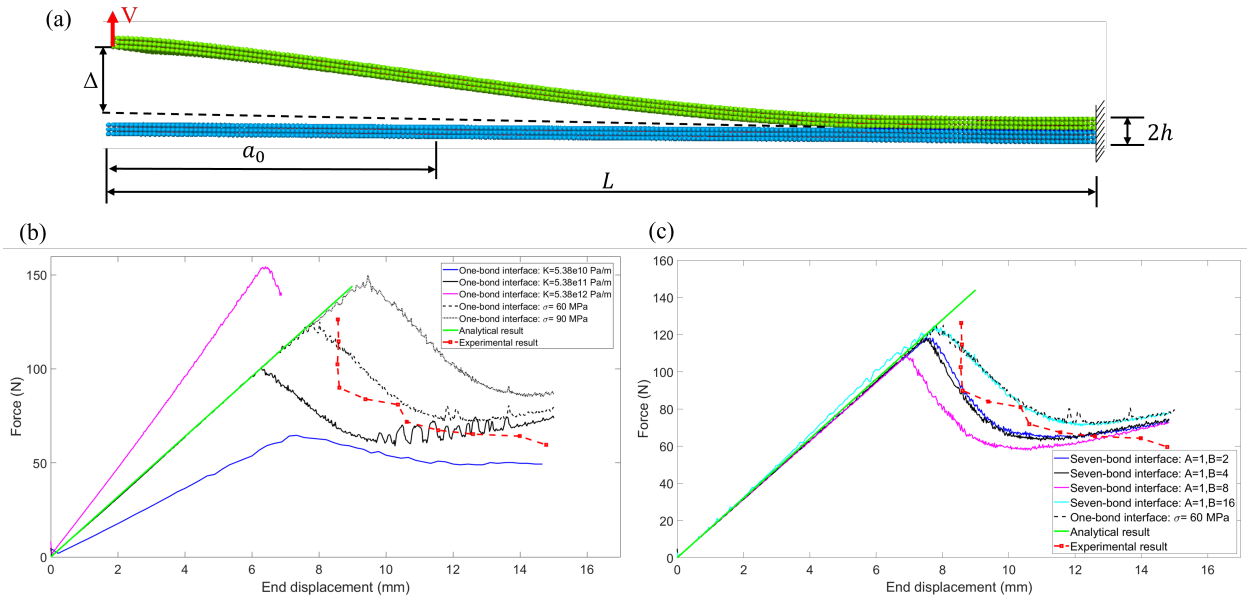

Figure 10: (a) schematic of FRMM test and comparison of load-displacement curves from (b) one-bond interface model and (c) seven-bond interface model.

models, the results from the model with A=1 and B=16 suggest the cracking of softening bonds initiated first due to their smallest bond strength at the end displacement of around 3 mm, while the primary bonds break at the end displacement of around 7.5 mm, compared to other models. The primary bonds in the model with A=1 and B=8 start break at the end displacement of 7 mm, indicating the lowest peak load found in 10(c). Interestingly, in the mixed-mode FRMM test, the primary bonds in the models with A=1, B=2 and A=1, B=4 break earlier than the ones with A=1 and B=16.

7. Conclusions

This study proposed a novel approach to deal with the softening behaviour at the ply-ply interface of composite materials. Based on the conservation of energy principle, a seven-bond interface model was proposed, in which two kinds of bonds, a primary bond and seven softening bonds, in one unit, were constructed, and the relation of energy between these bonds during cracking propagation was correlated with their lengths. Calibration of the stiffness of the interface of representative layers was conducted and compared with analytical and FEM

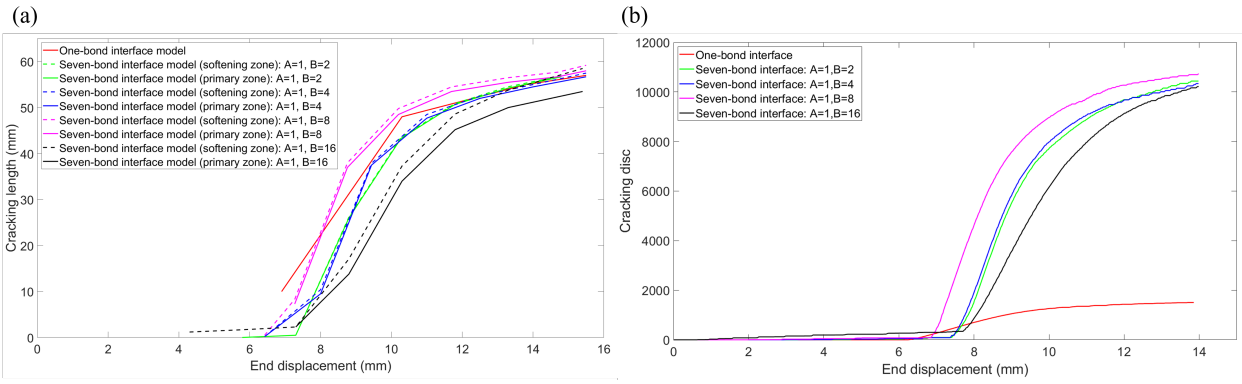

Figure 11: Comparisons of (a) cracking length - end displacement curves and (b) cracking disc number - end displacement of the FRMM test between one-bond and seven-bond interface models.

results. For simplicity, the same stiffnesses were used for the interface of the specimen and the strengths were determined from the elastic brittle constitutive model and the conservation of energy principle based on the power-law function. Three tests, including DCB, ELS and mixed-mode FRMM, were conducted and the results were compared to the experimental data and one-bond interface model. It was found that the seven-bond interface models with A=4, B=8, and A=1, B=8 and A=1, B=2 have a good agreement with the corresponding experimental data, i.e., the force-displacement and cracking length-displacement curves, in the DCB, ELS and FRMM tests, respectively. Notably, these parameters are only suitable for the selected cases and materials. They are not versatile but could be easily adjusted with DCB, ELS and FRMM tests. The main advantages of the proposed approach lie in its simplicity of implementation and efficiency in computation, compared to exclusively used cohesive/softening bilinear model.

It is worth noting that the delamination phenomenon is complex, especially when fibre bridging is involved. This is due to the interaction between the delamination and other intralaminar damage modes such as fibre breakage, matrix cracking and fibre/matrix interface debonding, which influences the damage progression in the composite laminates. Depending on the strengths of the fibre/matrix interface and interlaminar interface, the delamination could involve the fibre bridging when the fibre/matrix debonding is triggered. Therefore, in the future it is worth investigating the progressive damage in composites considering the

damage interaction with the proposed seven-bond interface bond model.

References

[1] E. F. Rybicki, M. F. Kanninen, A finite element calculation of stress intensity factors by a modified crack closure integral, Engineering Fracture Mechanics 9 (4) (1977) 931–938.

[2] R. Krueger, Virtual crack closure technique: history, approach, and applications, Applied Mechanics Reviews 57 (2) (2004) 109–143.

[3] C. Yang, A. Chadegani, J. S. Tomblin, Strain energy release rate determination of prescribed cracks in adhesively-bonded single-lap composite joints with thick bondlines, Composites Part B: Engineering 39 (5) (2008) 863–873.

[4] P. F. Liu, S. J. Hou, J. K. Chu, X. Y. Hu, C. L. Zhou, Y. L. Liu, J. Y. Zheng, A. Zhao, L. Yan, Finite element analysis of postbuckling and delamination of composite laminates using virtual crack closure technique, Composite Structures 93 (6) (2011) 1549–1560.

[5] R. Borg, L. Nilsson, K. Simonsson, Simulation of delamination in fiber composites with a discrete cohesive failure model, Composites Science and Technology 61 (5) (2001) 667–677.

[6] Q. Yang, B. Cox, Cohesive models for damage evolution in laminated composites, International Journal of Fracture 133 (2) (2005) 107–137.

[7] P. F. Liu, M. M. Islam, A nonlinear cohesive model for mixed-mode delamination of composite laminates, Composite Structures 106 (2013) 47–56.

[8] L. Zhao, Y. Gong, J. Zhang, Y. Chen, B. Fei, Simulation of delamination growth in multidirectional laminates under mode i and mixed mode i/ii loadings using cohesive elements, Composite Structures 116 (2014) 509–522.

[9] D. Xie, A. M. Waas, Discrete cohesive zone model for mixed-mode fracture using finite element analysis, Engineering Fracture Mechanics 73 (13) (2006) 1783–1796.

[10] X. Liu, R. Duddu, H. Waisman, Discrete damage zone model for fracture initiation and propagation, Engineering Fracture Mechanics 92 (2012) 1–18.

[11] P. F. Liu, J. Y. Zheng, Recent developments on damage modeling and finite element analysis for composite laminates: A review, Materials and Design 31 (8) (2010) 3825–3834.

[12] M. Elices, G. V. Guinea, J. Gomez, J. Planas, The cohesive zone model: advantages, limitations and challenges, Engineering Fracture Mechanics 69 (2) (2002) 137–163.

[13] W. Leclerc, H. Haddad, M. Guessasma, On the suitability of a Discrete Element Method to simulate cracks initiation and propagation in heterogeneous media, International Journal of Solids and Structures 108 (2017) 98–114.

[14] S. Silling, Reformulation of elasticity theory for discontinuities and long-range forces, Journal of the Mechanics and Physics of Solids 48 (1) (2000) 175–209.

[15] H. Ren, X. Zhuang, Y. Cai, T. Rabczuk, Dual-horizon peridynamics, International Journal for Numerical Methods in Engineering 108 (12) (2016) 1451–1476.

[16] P. A. Cundall, O. D. L. Strack, A discrete numerical model for granular assemblies, Géotechnique 29 (1) (1979) 47–65.

[17] P. W. Cleary, C. S. Campbell, Self-lubrication for Long Runout Landslides: Examination by computer simulation, Journal of Geophysical Research: Solid Earth 98 (B12) (1993) 21911–21924.

[18] B. LE, F. Dau, D. Pham, T. Tran, Discrete element modeling of interface debonding behavior in composite material: Application to a fragmentation test, Composite Structures 272 (2021) 114170.

[19] F. K. Wittel, J. Schulte-Fischedick, F. Kun, B.-H. Kröplin, M. Frieß, Discrete element simulation of transverse cracking during the pyrolysis of carbon fibre reinforced plastics to carbon/carbon composites, Computational materials science 28 (1) (2003) 1–15.

[20] Y. Sheng, D. Yang, Y. Tan, J. Ye, Microstructure effects on transverse cracking in composite laminae by DEM, Composites Science and Technology 70 (14) (2010) 2093–2101.

[21] D. Yang, Y. Sheng, J. Ye, Y. Tan, Dynamic simulation of crack initiation and propagation in cross-ply laminates by dem, Composites Science and Technology 71 (11) (2011) 1410–1418.

[22] Y. Ismail, Y. Sheng, D. Yang, J. Ye, Discrete element modelling of unidirectional fibre-reinforced polymers under transverse tension, Composites Part B: Engineering 73 (2015) 118–125.

[23] L. Wan, Y. Ismail, Y. Sheng, K. Wu, D. Yang, Progressive failure analysis of cfrp composite laminates under uniaxial tension using a discrete element method, Journal of Composite Materials 55 (8) (2021) 1091–1108.

[24] D. Yang, J. Ye, Y. Tan, Y. Sheng, Modeling progressive delamination of laminated composites by discrete element method, Computational materials science 50 (3) (2011) 858–864.

[25] B. Le, F. Dau, J. Charles, I. Iordanoff, Modeling damages and cracks growth in composite with a 3D discrete element method, Composites Part B: Engineering 91 (2016) 615–630.

[26] D. André, I. Iordanoff, J. luc Charles, J. Néauport, Discrete element method to simulate continuous material by using the cohesive beam model, Computer Methods in Applied Mechanics and Engineering 213-216 (2012) 113–125.

[27] A. Ammar, W. Leclerc, M. Guessasma, N. Haddar, Discrete element approach to simulate debonding process in 3d short glass fibre composite materials: Application to pa6/gf30, Composite Structures 270 (2021) 114035.

[28] Y. Hu, N. De Carvalho, E. Madenci, Peridynamic modeling of delamination growth in composite laminates, Composite Structures 132 (2015) 610–620.

[29] E. Onate, F. Zárate, J. Miquel, M. Santasusana, M. A. Celigueta, F. Arrufat, R. Gandikota, K. Valiullin, L. Ring, A local constitutive model for the discrete element method. application to geomaterials and concrete, Computational particle mechanics 2 (2) (2015) 139–160.

[30] Y. Tan, D. Yang, Y. Sheng, Discrete element method (DEM) modeling of fracture and damage in the machining process of polycrystalline SiC, Journal of the European ceramic society 29 (6) (2009) 1029–1037.

[31] I. C. Group, Pfc (particle flow code in 2 and 3 dimensions), version 5.0 (user's manual) (2014).

[32] L. Wan, D. Yang, Y. Ismail, Y. Sheng, 3d particle models for composite laminates with anisotropic elasticity, Composites Part B: Engineering 149 (2018) 110–121.

[33] K. Liu, W. Liu, Application of discrete element method for continuum dynamic problems, Archive of Applied Mechanics 76 (3) (2006) 229–243.

[34] S. Lenci, Analysis of a crack at a weak interface, International Journal of Fracture 108 (3) (2001) 275–290.

[35] A. Carpinteri, P. Cornetti, N. Pugno, Edge debonding in FRP strengthened beams: Stress versus energy failure criteria, Engineering Structures 31 (10) (2009) 2436–2447.

[36] V. Mantič, L. Távara, A. Blázquez, E. Graciani, F. París, A linear elastic-brittle interface model: application for the onset and propagation of a fibre-matrix interface crack under biaxial transverse loads, International Journal of Fracture 195 (1) (2015) 15–38.

[37] B. Wan, M. A. Sutton, M. F. Petrou, K. A. Harries, N. Li, Investigation of bond between fiber reinforced polymer and concrete undergoing global mixed mode i/ii loading, Journal of Engineering Mechanics 130 (12) (2004) 1467–1475.

[38] J.-G. Dai, B.-L. Wan, H. Yokota, T. Ueda, Fracture criterion for carbon fiber reinforced polymer sheet to concrete interface subjected to coupled pull-out and push-off actions, Advances in Structural Engineering 12 (5) (2009) 663–682.

[39] A. Kinloch, Y. Wang, J. Williams, P. Yayla, The mixed-mode delamination of fibre composite materials, Composites science and technology 47 (3) (1993) 225–237.

[40] A. Cerioni, Simulation of delamination in composite materials under static and fatigue loading by cohesive zone models, Ph.D. thesis, Universita'degli Studi di Cagliari (2009).

[41] P. P. Camanho, C. G. Davila, M. F. de Moura, Numerical simulation of mixed-mode progressive delamination in composite materials, Journal of Composite Materials 37 (16) (2003) 1415–1438.

[42] J. Chen, M. Crisfield, A. Kinloch, E. Busso, F. Matthews, Y. Qiu, Predicting progressive delamination of composite material specimens via interface elements, Mechanics of composite materials and structures 6 (4) (1999) 301–317.